1,3 Dichloro- and 1,3 dibromotetra-*n*-butyldistannoxane mixtures: ligand redistribution and fluxional dynamics in distannoxanes

David L. Tierney [a,1], Peter J. Moehs [a], Dennis L. Hasha [b,*]

[a] *Department of Chemistry, Saginaw Valley State University, University Center, MI 48710, USA*
[b] *Department of Chemistry, University of Missouri-Rolla, 142 Schrenk Hall, Rolla, MO 65409-0010, USA*

Abstract

The halogen redistribution reaction in the binary [$^nBu_2SnCl]_2O$/[$^nBu_2SnBr]_2O$ system is examined by ^{119}Sn- and ^{13}C-NMR spectroscopy. Binary mixtures of [$^nBu_2SnCl]_2O$ and [$^nBu_2SnBr]_2O$ reach equilibrium rapidly at room temperature. The reactant dimers are found to be in equilibrium with all five possible mixed distannoxane dimers in the equimolar mixture. These mixed distannoxane dimers differ in the ratio of Cl and Br as well as the relative positioning of the halogens. The mechanism responsible for the rapid formation of the mixed Cl:Br distannoxane dimers is found to proceed via bimolecular collisions producing a four-centered transition state, which in turn undergoes a concerted exchange of the halogens. The equilibrium concentrations of the reactant and product dimers are well represented by a statistical distribution, indicating that Cl and Br exhibit equivalent donor abilities. At 298 K, the NMR spectral data are consistent with time-averaged structures arising from rapidly interconverting rigid ladder pairs. Lowering the temperature to 173 K failed to freeze out this fluxional process. A reversible configurational rearrangement is also observed in which rotation about the oxygen–exocyclic tin bond results in the mutual exchange of halogens associated with the same exocyclic tin atom. © 2001 Elsevier Science B.V. All rights reserved.

Keywords: Tin; Distannoxane; Rearrangement; Redistribution; NMR

1. Introduction

Tetraorganodistannoxanes have been used to catalyze the polymerizations of ethylene oxide [1], ethylene terephthalate [2], urethanes [3] and butyrolactone [4]. Tetraorganodistannoxanes have also been instrumental in cross-linking room temperature-vulcanized (RTV) silicone elastomers [5] and catalyzing chemical modifications [6] of immiscible polymer blends resulting in improved compatibility [7]. In addition, these important catalytic compounds have been shown to exhibit in vitro activity against leukemia [8] and various cancer tumor cell lines [9], as well as in the control of phytopathogenic fungi and bacteria [10]. Structurally, vapor-phase osmometry studies [11–16], cyroscopic measurements [16–19], IR [19,20] and ^{119}Sn-NMR [7c,7f,9,12,21–32] spectroscopy have demonstrated that this important class of compounds exists as dimers in nonpolar solvents. In 1963, Okawara and Wada [17] proposed that in solution the tetraorganodistannoxanes are represented by a dimeric ladder structure. Subsequent X-ray analyses have shown that the ladder structure is the predominant structure adopted in the solid state [9,28–37]. The tin, oxygen and bridging X ligands of the ladder structure are essentially coplanar. Each tin possesses two pendent organic groups; however, for the purpose of clarity these have been omitted. The ladder
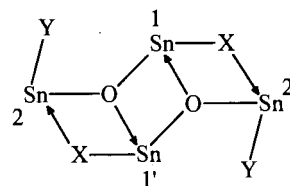
---

structure contains two distinct pentacoordinated tin environments, designated as endocyclic, Sn(1) and Sn(1′), and exocyclic, Sn(2) and Sn(2′). The endocyclic tin atoms are located within the four-membered ring containing the two oxygens and attached to these ring oxygens are the exocyclic tin atoms. The geometries of the endocyclic and exocyclic tin atoms are distorted *cis*-R_2SnXYZ trigonal bipyramids.

In solution, the ^{119}Sn-NMR spectra of monofunctional tetraorganodistannoxanes, $\{[R_2SnX]_2O\}_2$, contain two resonances with chemical shifts consistent with pentacoordinated tin environments, -60 to -235 ppm [7c,9,21–32]. With few exceptions, the mixed tetraorganodistannes, $\{YR_2SnOSnR_2X\}_2$ (Y = Cl, Br, I, NCS; Y = OH, alkoxy, phenoxy) [22,23], studied thus far, also yield two tin resonances in the same spectral region. The ladder structure for monofunctional tetraorganodistannoxanes (X = Y) has been observed to undergo a dynamic process [28,30] involving interconverting ladder structures. This fluxional process designated the intradimeric distannoxane process [27], yields time-averaged NMR spectra. The observed chemical shifts and scalar couplings of $\{[R_2SnX]_2O\}_2$, are simple averages of the individual ladder values. For mixed distannoxanes, $\{YR_2SnOSnR_2X\}_2$, this fluxional process has been suggested to be inoperative, resulting in a single frozen dimer with the better donor ligand occupying the bridging sites [27].

The exceptions to the ubiquitous two-line ^{119}Sn-NMR spectra are the $[^nBu_2SnCl]_2O/[^nBu_2Sn(O_2CCH_3)]_2O$ [24] and $[^nBu_2SnF]_2O/[^nBu_2Sn(O_2CR)]_2O$, (R = CH_3, ^tBu and Ph) [25], binary systems. In the equimolar mixture of $[^nBu_2SnCl]_2O$ and $[^nBu_2Sn(O_2CCH_3)]_2O$, the 18 reported ^{119}Sn resonances were interpreted using ladder structures with the acetoxy ligand preferentially occupying the bridging sites [24]. Using ladder structures, Jain and coworkers [25] identified similar F-bridged products in the binary mixtures of $[^nBu_2SnF]_2O/[^nBu_2Sn(O_2CR)]_2O$, (R = CH_3, ^tBu and Ph). Gross suggested that formation of the mixed distannoxane dimers takes place by dissociation of the dimers and subsequent ligand exchange among monomeric species [24]. However, for metal complexes, it is generally believed that ligand redistribution occurs via bimolecular collisions producing a four-centered transition state, which in turn undergoes a concerted swap of the ligands [38–41]. In the case of tin(IV) halides, R_2SnX_2, a dissociative mechanism, in which labile halides catalyze the exchange, is responsible for the redistribution of the halogens [42].

In this paper, ^{119}Sn- and ^{13}C-NMR spectroscopy is employed to examine the reaction products, fluxional dynamics and halogen redistribution mechanism for the $[^nBu_2SnCl]_2O/[^nBu_2SnBr]_2O$ binary system.

2. Experimental

2.1. Chemicals

Di-*n*-butyltin dichloride and di-*n*-butyltin oxide were obtained from Strem Chemicals and used without further purification. Di-*n*-butyltin dibromide was prepared according to literature methods [43,44] from concentrated HBr and di-*n*-butyltin oxide. All of the solvents used in this study were newly acquired and possessed one of the following purity designations: NMR, HPLC or analytical grade.

2.2. Preparation of $[^nBu_2SnCl]_2O$

A solution containing 30.4 g di-*n*-butyltin dichloride and 100 g methylene dichloride was added to 2.0 l of deionized water and mixed vigorously. The extent of the reaction was monitored by continuous measurement of the pH in the aqueous layer. When the pH approached the theoretical end-point, 1.30, signaling the completion of the reaction, the organic layer was separated and dried over sodium sulfate. The solid product obtained from solvent evaporation was then recrystallized from *t*-amyl alcohol. This procedure afforded 1,3-dichlorotetra-*n*-butyldistannoxane in 93% yield; m.p.: 111–113°C. NMR (1.0 M in $CDCl_3$) ^{119}Sn, -92.0, -140.6 ppm; $(^{\alpha}CH_2^{\beta}CH_2^{\gamma}CH_2^{\delta}CH_3)$ ^{13}C (from ^{13}C 2D INADEQUATE) 32.8 (α-*endo*), 32.2 (α-*exo*), 27.3 (β-*exo*), 27.1 (β-*endo*), 26.5 (γ-*endo*), 26.4 (γ-*exo*), 13.6 (δ-*endo*), 13.5 ppm (δ-*exo*); $^1J(^{119}Sn(endo), {}^{\alpha}C) = 594$, $^1J(^{119}Sn(exo), {}^{\alpha}C) = 569$, $^2J(^{119}Sn(endo), {}^{\beta}C) = 34.4$, $^2J(^{119}Sn(exo), {}^{\beta}C) = 30.7$, $^3J(^{119}Sn(endo), {}^{\gamma}C) = 119$, $^3J(^{119}Sn(exo), {}^{\gamma}C) = 107$ Hz; ^1H (from 2D ^1H–^{13}C heteronuclear correlation (HETCOR)) 1.83 (β-*endo*), 1.80 (β-*exo*), 1.78 (α-*endo*), 1.76 (α-*exo*), 1.43 (γ-*endo*), 1.39 (γ-*exo*), 0.96 (δ-*endo*), 0.95 ppm (δ-*exo*), $^2J(^{119}Sn(endo), {}^{\alpha}H) = 76$, $^2J(^{119}Sn(exo), {}^{\alpha}H) = 74$, $^3J(^{119}Sn(endo), {}^{\beta}H) = 81$, $^3J(^{119}Sn(exo), {}^{\beta}H) = 101$ Hz. Anal. Calc. for $[^nBu_2SnCl]_2O$: C, 34.73; H, 6.56. Found: C, 34.52; H, 6.46%.

2.3. Preparation of $[^nBu_2SnBr]_2O$

Synthesis of $[^nBu_2SnBr]_2O$ was carried out by the aqueous hydrolysis of di-*n*-butyltin dibromide using the same procedure described for the synthesis of $[^nBu_2SnCl]_2O$ with a yield of 72%; m.p.: 108–110°C. NMR (1.0 M in $CDCl_3$) ^{119}Sn, -83.1, -132.2 ppm; $(^{\alpha}CH_2^{\beta}CH_2^{\gamma}CH_2^{\delta}CH_3)$ ^{13}C (from ^{13}C 2D INADEQUATE) 36.2 (α-*endo*), 36.0 (α-*exo*), 27.7 (β-*exo*), 27.2 (β-*endo*), 26.5 (γ-*endo*), 26.3 (γ-*exo*), 13.6 (δ-*endo*), 13.5 ppm (δ-*exo*); $^1J(^{119}Sn(endo), {}^{\alpha}C) = 595$, $^1J(^{119}Sn(exo), {}^{\alpha}C) = 547$, $^2J(^{119}Sn(endo), {}^{\beta}C) = 33.9$, $^2J(^{119}Sn(exo), {}^{\beta}C) = 31.0$, $^3J(^{119}Sn(endo), {}^{\gamma}C) = 139$, $^3J(^{119}Sn(exo), {}^{\gamma}C) = 105$ Hz; ^1H (from 2D ^1H–^{13}C heteronuclear cor-

relation (HETCOR)) 1.93 (α-*endo*) 1.87 (α-*exo*), 1.85 (β-*endo*), 1.81 (β-*exo*), 1.41 (γ-*endo*), 1.39 (γ-*exo*), 0.95 (δ-*endo*), 0.94 ppm (δ-*exo*), $^2J(^{119}Sn(endo), \, ^{\alpha}H) = 89$, $^2J(^{119}Sn(exo), \, ^{\alpha}H) = 73$, $^3J(^{119}Sn(endo), \, ^{\beta}H) = 85$, $^3J(^{119}Sn(exo), \, ^{\beta}H) = 105$ Hz. Anal. Calc. for [$^nBu_2SnBr]_2O$: C, 29.92; H, 5.65. Found: C, 30.51; H, 5.78%.

2.4. Binary mixtures

Binary mixtures of [$^nBu_2SnCl]_2O$ and [$^nBu_2SnBr]_2O$, with approximate mol ratios 10:1, 3:1, 1:1, 1:3 and 1:10 ([$^nBu_2SnCl]_2O$:[$^nBu_2SnBr]_2O$), were prepared by dissolving the appropriate amount of distannoxanes in 0.5 ml benzene-d_6. The desired quantities of [$^nBu_2SnCl]_2O$ and [$^nBu_2SnBr]_2O$ were determined by constraining the total tin concentration of each of the solutions to $[Sn]_T = 2.0$ M.

2.5. NMR spectra

149.21 MHz ^{119}Sn MAS-NMR solid-state spectra were acquired with high power proton decoupling at various spin rates between 3.5 and 7.0 kHz, using a Bruker MSL400 NMR spectrometer. The solid-state spectra were referenced using external $(CH_3)_4Sn$ (TMT = 0.0 ppm). The principal elements of the shielding tensors, σ_{11}, σ_{22}, and σ_{33}, are extracted using HBA [45]. The HBA computer program analyzes the intensities of the spinning sidebands using the method of Herzfeld and Berger [46]. The accuracy of δ_{iso}, Ω (and ζ), κ (and η) corresponds to ± 0.05 ppm (digital resolution), ± 10 ppm and ± 0.05, respectively. 111.96 MHz ^{119}Sn-, 75.51 MHz ^{13}C- and 300.14 MHz ^1H-NMR spectra of solutions containing [$^nBu_2SnCl]_2O$ and [$^nBu_2SnBr]_2O$ were obtained using Varian INOVA 300 and 400 NMR spectrometers. The ^{119}Sn-NMR spectra were referenced with internal tetramethyltin (TMT = 0.0 ppm); while tetramethylsilane (TMS = 0.0 ppm) was used to reference the ^{13}C- and ^1H-NMR spectra. Quantitation of the tin spectra were assured by using a recycle time of 1.5 s which is significantly longer than the observed spin-lattice relaxation times, 80–130 ms. The ^{119}Sn 1D and 2D INADEQUATE experiments were optimized for $J(^{119}Sn, \, ^{119}Sn) = 60$ Hz.

The ^{13}C 2D chemical exchange (EXSY) experiment was conducted at 328 K, on the 1:1 [$^nBu_2SnCl]_2O$/[$^nBu_2SnBr]_2O$ mixture in benzene-d_6 with the mixing period set to 0.5 and 1 s. Using the same experimental conditions, ^{13}C EXSY spectra were also obtained on the same solution after the addition of 23, 46, 78 and 190 mg of iodine ([I_2] = 0.03–0.25 M). ^{119}Sn EXSY experiments were performed on the equimolar [$^nBu_2SnCl]_2O$/[$^nBu_2SnBr]_2O$ mixture in two solvents, benzene-d_6 and CDCl$_3$, as a function of temperature, 298–348 K. Rate constants are obtained by fitting the observed integrated volumes of the two-dimensional spectra to the kinetic parameters of the rate matrix, **L**. The off-diagonal elements of the rate matrix, L_{ji}, are given by the rate constants, $-k_{ij}$, associated with magnetization transfer from site i to j. The 2D volume matrix, **I**, is related to **L** by

$$\mathbf{L} = \frac{\ln(\mathbf{P}^{-1}\mathbf{I})}{\tau_m} = \frac{\ln \mathbf{J}}{\tau_m},$$

where **J** is the normalized volume matrix and **P** is the volume matrix at $\tau_m = 0$. The elements of the diagonal matrix **P** are proportional to the equilibrium populations. The off-diagonal elements of **L**, which are the off-diagonal elements of ln **J**, are readily calculated via matrix diagonalization of **J** [47–51]. For a given temperature, up to eight spectra were obtained; one at $\tau_m = 0$ and the others at mixing times centered near the optimum ($0.5\tau_m(opt)$ to $2\tau_m(opt)$; $\tau_m(opt) \approx 1/\{(1/T_1) + k_{ij} + k_{ji}\}$ [52,53]). The reported rate constants are mean values, $k_{ij} = \langle k_{ij} \rangle$, with variance given by $\sigma^2(k_{ij}) = \Sigma_m(k_{ij}(\tau_m) - k_{ij})^2/(N-1)$, where N is the number of spectra acquired with $\tau_m > 0$. The variance, $\sigma^2(k_{ij})$, is found to be significantly larger than the variance in the mean determined from rms noise of the individual experiments, $1/\Sigma(1/\sigma^2(k_{ij}))$. The reported errors in the rate constants, as well as the activation parameters represent an estimate of the 95% confidence level.

3. Results and discussion

3.1. ^{119}Sn-NMR spectrum

The 149.21 MHz ^{119}Sn MAS-NMR solid-state spectra of [$^nBu_2SnCl]_2O$ and [$^nBu_2SnBr]_2O$ (Fig. 1) are dominated by chemical shift anisotropy (CSA). Both spectra consist of two spinning sideband manifolds that trace out extremely large asymmetric CSA patterns, approximately 1000 ppm in breadth. Each CSA pattern is comprised of a single isotropic resonance flanked by spinning sidebands that are separated by the sample rotation frequency. By varying the speed of sample rotation, the isotropic chemical shifts associated with the two tin environments are readily identified: $\{[^nBu_2SnCl]_2O\}_2$, $\delta_{iso} = -76.8$ and -140.2 ppm, and $\{[^nBu_2SnBr]_2O\}_2$, $\delta_{iso} = -56.0$ and -134.4 ppm. The observed isotropic chemical shifts are consistent with the pentacoordinated tin environments of the dimeric ladder structure. The principal elements of the shielding tensors, σ_{11}, σ_{22}, and σ_{33}, as well as their derivative functions, Ω and κ [54] (or alternatively, ζ and η) [55], for $\{[^nBu_2SnCl]_2O\}_2$ and $\{[^nBu_2SnBr]_2O\}_2$ are not only comparable to the values reported for the pentacoordinated tins of $\{[(CH_3)_2Sn(O_2CR)]_2O\}_2$ (R = CH$_3$, *p*-toluene, C$_6$F$_5$, *t*-butyl) but also the hexacoordinated tins of $\{[(CH_3)_2Sn(O_2CR)]_2O\}_2$ (R = CH$_3$ and *t*-butyl) [32]

(Table 1). The span, $\Omega = \sigma_{33} - \sigma_{11}$, defines the overall breadth of the CSA pattern; while the skew, $\kappa = 3(\sigma_{iso} - \sigma_{22})/\Omega$, is a measure of the axial anisotropy. When $\kappa = \pm 1$, the symmetry of the chemical shielding tensor is described by prolate or oblate ellipsoids, respectively; while axial symmetry in the chemical shielding tensor is absent when $\kappa = 0$ [54]. The spans associated with the chemical shielding tensors for the two tin sites of $\{[^n Bu_2 SnCl]_2 O\}_2$ and $\{[^n Bu_2 SnBr]_2 O\}_2$ define the range for the tetraorganodistannoxanes studied thus far, 995–1447 ppm. For the three unambiguously assigned distannoxanes, $\{[^n Bu_2 SnCl]_2 O\}_2$, $\{[^n Bu_2 SnBr]_2 O\}_2$ and $\{[(CH_3)_2 Sn(O_2 C^t Bu)]_2 O\}_2$, it is observed that Ω (*endo*) $> \Omega$ (*exo*) by 88–320 ppm. The skew values for the tetraorganodistannoxanes are observed to be positive, $\kappa = 0.16$, 0.33–0.50. Smaller values of κ, yet still positive, are found for the pentacoordinated tin atoms of polymeric $R_2 SnO$, $\kappa((CH_3)_2 SnO) = 0.08$ [56,57] and $\kappa(^n Bu_2 SnO) = 0.13$ [56–58], indicating a near total lack of axial symmetry. The polymeric $R_2 SnO$ lattice, which consists of interconnected $R_2 SnOSnR_2 O$ four-membered rings, possesses tin atoms with nearly ideal *cis*-$R_2 SnX_3$ geometries [59,60]. The CSA patterns due to the nearly ideal $R_2 SnO$ geometries exhibit significantly smaller spans compared to the tetraorganodistannoxanes; $\Omega((CH_3)_2 SnO) = 762$ ppm [57,58] and $\Omega(^n Bu_2 SnO) = 737$ ppm [56–58]. The increased span and larger skew of the CSA patterns associated with the tetraorganodistannoxanes are due to distortions from ideal *cis*-$R_2 SnX_3$ trigonal bipyramidal geometry. These distortions may be due to the constraints imposed by the fused ring system as well as possible weak interactions between the tin and ligand atoms at distances less

than the van der Waal radii sum [33]. For example, in $[(CH_3)_2 SnCl]_2 O$ the internuclear distance between the endocyclic tin atom and proximal nonbridging Cl is 3.409 Å; while the exocyclic tin atom and bridging Cl belonging to an adjacent dimer are 3.339 Å apart [32,34]. These additional long-range interactions, which suggest a possible increase in coordination number from 5 to 6, may explain the similarity in the CSA patterns of the pentacoordinated and hexacoordinated tin atoms found in tetraorganodistannoxanes.

In noncoordinating solvents, $[^n Bu_2 SnCl]_2 O$ and $[^n Bu_2 SnBr]_2 O$ produce ^{119}Sn resonances with chemical shifts comparable to those observed for the solids: $\{[^n Bu_2 SnCl]_2 O\}_2$, -89.6 and -142.3 ppm; $\{[^n Bu_2 SnBr]_2 O\}_2$, -82.7 and -133.7 ppm (0.25 M in benzene-d_6). Similar chemical shifts for both phases indicate that the solution and solid-state structures are closely related [27,31,32], confirming that $\{[^n Bu_2 SnCl]_2 O\}_2$ and $\{[^n Bu_2 SnBr]_2 O\}_2$ are well represented by the dimeric ladder structure of the solid state. Based on the relative number of halogens attached to the endo- and exocyclic tins of $\{[R_2 SnX]_2 O\}_2$ (X = Cl, Br) and $\{YR_2 SnOSnR_2 OR'\}_2$ (Y = Cl, Br; R' = H, phenyl), Otera et al. [22] assigned the high frequency resonance to the exocyclic tin environment. The tin resonances of $\{[^n Bu_2 SnCl]_2 O\}_2$ and $\{[^n Bu_2 SnBr]_2 O\}_2$ exhibit satellites due to tin–carbon and tin–tin couplings (Fig. 2). The exo- and endocyclic tin resonances for both $\{[^n Bu_2 SnCl]_2 O\}_2$ and $\{[^n Bu_2 SnBr]_2 O\}_2$ possess an intense satellite pair with a common splitting of 72 and 78 Hz, respectively. These satellites are due to unresolved $^{119}Sn–^{119}Sn$ and $^{119}Sn–^{117}Sn$ couplings between the exo- and endocyclic tins, $^2J(exo,endo)$, and are equal to previously reported values [23,27]. Although a single $^2J(endo,exo)$ is observed for $\{[^n Bu_2 SnCl]_2 O\}_2$, $\{[^n Bu_2 SnBr]_2 O\}_2$ and $\{[^n Bu_2 SnX]_2 O\}_2$ (X = OR, O_2CR) [7c,7f,9,23,27,30–32], ladder structures are expected to possess two possible exo–endocyclic tin couplings, $^2J(1,2)$ and $^2J(1,2')$. Deconvolution of the $\{[^n Bu_2 SnCl]_2 O\}_2$ and $\{[^n Bu_2 SnBr]_2 O\}_2$ spectra reveals that the integrated intensity of these satellites relative to the main line, are twice the expected sum of the natural abundance of ^{119}Sn and ^{117}Sn. This observation indicates that $^2J(1,2)$ and $^2J(1,2')$ are either fortuitously coincidental [23] or equivalent due to averaging caused by the intradimeric distannoxane process [27]. For $\{[^n Bu_2 SnBr]_2 O\}_2$ weaker satellite pairs with different splittings 34.5 Hz (*exo*) and 42.4 Hz (*endo*) are observed; while satellites with similar splittings for $\{[^n Bu_2 SnCl]_2 O\}_2$ are observed only with the assistance of resolution enhancement, 30.9 (*exo*) and 21.4 Hz (*endo*). The ^{119}Sn INADEQUATE experiment, which identifies $^{119}Sn–^{119}Sn$ pairs, is unable to detect these weaker satellites indicating that the splittings arise from $^{119}Sn–^{117}Sn$ couplings involving identical tin environ-

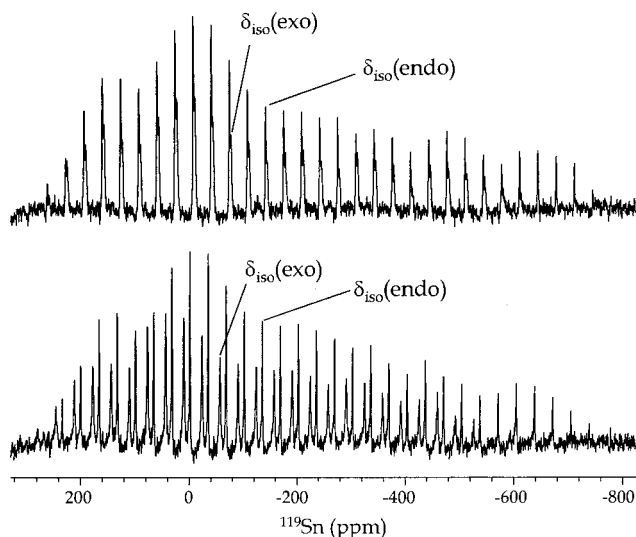Fig. 1. 149.21 MHz ^{119}Sn MAS-NMR spectra of $\{[^n Bu_2 SnCl]_2 O\}_2$ (top) and $\{[^n Bu_2 SnBr]_2 O\}_2$ (bottom) obtained at a spinning rate of 4.5 kHz. Recycle time, 30 s; 64 transients.

Table 1
^{119}Sn solid-state-NMR spectral data of tetraorganodistannoxanes

Compound	Assignment	CN [a]	δ_{iso} (ppm) [b]	σ_{11} (ppm) [b]	σ_{22} (ppm) [b]	σ_{33} (ppm) [b]	Ω (ppm) [c]	κ [c]	ζ (ppm) [d]	η [d]
[^{n}Bu$_2$SnCl]$_2$O [e]	Exocyclic	5	−76.8	−409	−79	718	1127	0.41	641	0.51
	Endocyclic	5	−140.2	−464	−99	983	1447	0.50	843	0.43
[^{n}Bu$_2$SnBr]$_2$O [e]	Exocyclic	5	−56.0	−384	−59	611	995	0.35	555	0.59
	Endocyclic	5	−134.4	−369	−11	783	1152	0.38	649	0.55
[Me$_2$Sn(O$_2$CR)]$_2$O [f]	Endo (or exo) [g]	5	−177	−280	4	807	1087	0.48	630	0.45
R = C$_6$F$_5$	Exo (or endo)	5	−219	−331	59	929	1260	0.38	710	0.55
[Me$_2$Sn(O$_2$CR)]$_2$O [f]	Endo (or exo) [g]	5	−195	−335	82	838	1173	0.29	643	0.65
R = p-toluene	Exo (or endo)	5	−233	−249	112	836	1085	0.33	603	0.60
[Me$_2$Sn(O$_2$CR)]$_2$O [f]	Exocyclic	5	−184	−349	140	760	1087	0.48	576	0.49[h]
R = ^{t}Bu	Endocyclic	6	−267	−184	74	911	1260	0.38	644	0.60[h]
[Me$_2$Sn(O$_2$CR)]$_2$O [f]	Endo (or exo) [g]	5	−178	−316	55	795	1111	0.33	617	0.60
R = CH$_3$	Exo (or endo)	5	−209	−334	149	812	1146	0.16	603	0.80
	Endo (or exo)	6	−287	−140	57	944	1084	0.64	657	0.30
	Exo (or endo)	6	−298	−155	54	995	1150	0.64	697	0.30

[a] CN, coordination number.

[b] $\delta_{iso} = -\sigma_{iso} = -(\sigma_{11} + \sigma_{22} + \sigma_{33})/3$; $\sigma_{33} \geq \sigma_{22} \geq \sigma_{11}$.

[c] Convention proposed by Mason [54]. $\Omega(\text{span}) = \sigma_{33} - \sigma_{11}$; $\kappa(\text{skew}) = 3(\sigma_{iso} - \sigma_{22})/\Omega$. κ corresponds to the parameter ρ used in the Herzfeld–Berger analysis; while Ω is related to the Herzfeld–Berger μ parameter ($\Omega = \mu v_{rot}/v_o$, where v_{rot} is the spinning rate and v_o is the spectrometer frequency in MHz) [46].

[d] Haeberlen–Mehring [55] convention: $|\sigma_{ZZ} - \sigma_{iso}| \geq |\sigma_{XX} - \sigma_{iso}| \geq |\sigma_{YY} - \sigma_{iso}|$; $\zeta(\text{anisotropy}) = \sigma_{11} - \sigma_{iso} < 0$ (for $\sigma_{ZZ} = \sigma_{11}$) and $= \sigma_{33} - \sigma_{iso} > 0$ (for $\sigma_{ZZ} = \sigma_{33}$); $\eta(\text{asymmetry}) = (\sigma_{22} - \sigma_{33})/\zeta$ (for $\zeta < 0$) and $\eta = (\sigma_{22} - \sigma_{11})/\zeta$ (for $\zeta > 0$). For the chemical shielding tensors presented here $\sigma_{ZZ} = \sigma_{33}$, $\sigma_{YY} = \sigma_{22}$ and $\sigma_{XX} = \sigma_{11}$; $\zeta = \Omega + (\sigma_{11} - \sigma_{iso})$ and $\eta = \{\sigma_{iso} - (\sigma_{11} + \Omega\kappa/3)\}/\{\Omega + (\sigma_{11} - \sigma_{iso})\}$.

[e] This work.

[f] Ref. [32].

[g] Tentative assignments.

[h] The asymmetries, η, reported for [Me$_2$Sn(O$_2$C^{t}Bu)]$_2$O in Ref. [32] do not correspond to the experimentally determined values of the shielding tensor. The η-values presented here are recalculated from the principal elements of the shielding tensor in Ref. [32].

ments. This observation confirms that in solution $\{[^n\text{Bu}_2\text{SnCl}]_2\text{O}\}_2$ and $\{[^n\text{Bu}_2\text{SnBr}]_2\text{O}\}_2$ each possess a pair of chemically equivalent tin atoms for both endo- and exocyclic sites. These ^{119}Sn–^{117}Sn couplings, which are designated $^4J(exo,exo)$ and $^2J(endo,endo)$, fall in the range previously reported for $\{[^n\text{Bu}_2\text{SnCl}]_2\text{O}\}_2$ [27], $\{[^n\text{Bu}_2\text{Sn}(\text{O}_2\text{CCH}_3)]_2\text{O}\}_2$ [27] and $\{\text{Cl}^n\text{BuSnOSn}^n\text{Bu-OH}\}_2$ [61]. The observed magnitudes of $^4J(exo,exo)$ are similar to the four-bond coupling, $^4J(^{119}\text{Sn},^{117}\text{Sn}) = 44$ Hz, detected in the sterically congested (neophyl$_3$-Sn)$_2$CO$_3$ (neophyl = C$_6$H$_5$(CH$_3$)$_2$CCH$_2$–) [62]. The small couplings between endocyclic tins which operate through the Sn(1)OSn(1′)O constrained four-membered ring, can be explained using a simple Fermi contact model [63]. In this model, the magnitude of the coupling constant is dependent on the s character of the tin–oxygen bond. Since the Sn–O–Sn bond angle in the constrained four-membered ring is approximately 105° [9,28–37], the tin–oxygen bond would be expected to contain insufficient s character to yield a sizeable coupling constant. Still weaker couplings to the α and γ carbons as well as satellites arising from coupling to two tin nuclei are also observed.

The spin–spin coupling responsible for the α-carbon satellites, $^1J(^{119}\text{Sn},^{13}\text{C})$, is diagnostic of tin coordination [64–69]. Mitchell [64] has reported that for dialkyltin compounds, the magnitude of $^1J(^{119}\text{Sn},^{13}\text{C})$ falls in the range of 370–480 Hz for tetracoordinated tin and 900–970 Hz for hexacoordinated tin. The magnitudes of $^1J(^{119}\text{Sn},^{13}\text{C})$ reported for several distannoxane dimers are intermediate indicating pentacoordinated tin environments, 510–820 Hz [7c,f,9,27,29,31,32]. For $\{[^n\text{Bu}_2\text{SnCl}]_2\text{O}\}_2$ and $\{[^n\text{Bu}_2\text{SnBr}]_2\text{O}\}_2$, the magnitudes of $^1J(^{119}\text{Sn},^{13}\text{C})$ associated with the endo- and exocyclic sites fall towards the low end of the distannoxane range: $^1J(^{119}\text{Sn}(endo),^{13}\text{C})$ is 601 and 602 Hz for $\{[^n\text{Bu}_2\text{SnCl}]_2\text{O}\}_2$ and $\{[^n\text{Bu}_2\text{SnBr}]_2\text{O}\}_2$, respectively; while the corresponding exocyclic couplings are slightly smaller, $^1J(^{119}\text{Sn}(exo),^{13}\text{C}) = 574$ and 552 Hz. The magnitude of $^1J(^{119}\text{Sn},^{13}\text{C})$ is linearly related to the C–Sn–C bond angle, θ [67–69]. Using the relationship developed specifically for di-n-butyltin(IV) compounds by Holeček and Lyčka [67], values of θ for $\{[^n\text{Bu}_2\text{SnCl}]_2\text{O}\}_2$ are 135° (endo) and 132° (exo); while for $\{[^n\text{Bu}_2\text{SnBr}]_2\text{O}\}_2$ θ values are 135° (endo) and 130° (exo). Although the correlation yields angles with an uncertainty of ± 4° [68], the relationship indicates that θ (exo) decreases slightly on going from Cl to the larger Br ligand; while θ (endo) remains virtually unchanged. Changing the solvent to a 2:1 mixture (by volume) of tetrachloroethylene and benzene-d_6, results in an increase in $^1J(^{119}\text{Sn},^{13}\text{C})$ associated with both sites of $\{[^n\text{Bu}_2\text{SnCl}]_2\text{O}\}_2$: $^1J(^{119}\text{Sn}(endo),^{13}\text{C}) = 605$ Hz and $^1J(^{119}\text{Sn}(exo),^{13}\text{C}) = 577$ Hz [27]; while changing the

solvent to $CDCl_3$ yields reduced $^1J(^{119}Sn,^{13}C)$ values: $^1J(^{119}Sn(endo),^{13}C) = 594$ Hz and $^1J(^{119}Sn(exo),^{13}C) = 569$ Hz.

The $[^nBu_2SnCl]_2O/[^nBu_2SnBr]_2O$ binary system reaches equilibrium rapidly at room temperature. The 111.96 MHz ^{119}Sn-NMR spectrum resulting from the addition of equimolar quantities of $[^nBu_2SnCl]_2O$ and $[^nBu_2SnBr]_2O$ in benzene-d_6, acquired at 298 K consists of 20 resonances (Fig. 3c). These resonances fall into two well-defined regions; one-half of the signals are located in the spectral region assigned to exocyclic tin atoms, -82 to -91 ppm, and the remaining resonances are observed in the low frequency region attributed to the endocyclic tin atoms, -129 and -149 ppm. The resonance pairs detected at -89.8, -142.6 and -82.9, -134.0 ppm indicate the presence of the reactant dimers, $\{[^nBu_2SnCl]_2O\}_2$ and $\{[^nBu_2SnBr]_2O\}_2$, respectively. The remaining 16 resonances can be ex-

Fig. 3. 111.96 MHz ^{119}Sn-NMR spectra of binary $[^nBu_2SnCl]_2O/[^nBu_2SnBr]_2O$ mixtures with $[Sn]_T = 2.0$ M in benzene-d_6 at 298 K. The spectra correspond to the following compositions ($[^nBu_2SnCl]_2O:[^nBu_2SnBr]_2O$): (a) 10:1; (b) 3:1; (c) 1:1; (d) 1:3 and (e) 1:10. **4Cl** = $\{[^nBu_2SnCl]_2O\}_2$; **4Br** = $\{[^nBu_2SnBr]_2O\}_2$; **I** = 3:1 (Cl:Br) mixed distannoxane dimer; **II** = 1:3 mixed distannoxane dimer and the eight resonances associated with the 2:2 mixed distannoxane dimers are denoted with asterisks.

Fig. 2. Expansion of the 111.96 MHz ^{119}Sn-NMR spectra of (a) 0.50 M $[^nBu_2SnCl]_2O$ and (b) 0.50 M $[^nBu_2SnBr]_2O$ solutions in benzene-d_6 at 298 K. Resolution enhancement of the $\{[^nBu_2SnCl]_2O\}_2$ spectrum is accomplished using a 15° phase shifted sinebell of fractional length 0.2. For the $\{[^nBu_2SnBr]_2O\}_2$ spectrum exponential apodization, 0.5 Hz linebroadening, is employed. The weak resonance denoted with an asterisk in the spectrum of $\{[^nBu_2SnBr]_2O\}_2$ is attributed to an unidentified impurity.
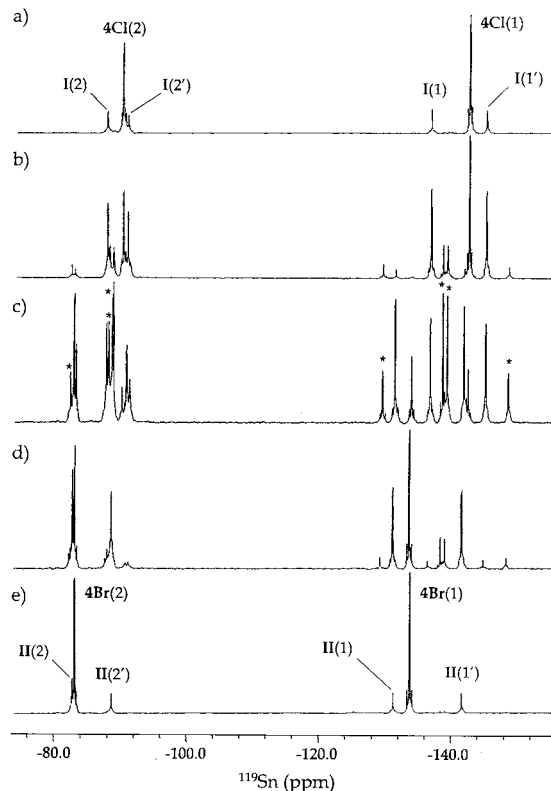
plained by assuming that the products are also dimers, which contain four tin atoms and four halogen ligands. These product dimers differ in the ratio of Cl and Br ligands as well as their relative positions. By varying the molar ratio of the reactant distannoxanes, the resonances due to the product dimers are readily identified. The ^{119}Sn-NMR spectrum of the 10:1 ($[^nBu_2SnCl]_2O/[^nBu_2SnBr]_2O$) (Fig. 3a) contains two intense resonances due to $\{[^nBu_2SnCl]_2O\}_2$ and four weaker resonances with equal intensity at -87.5, -90.6, -136.8 and -145.1 ppm. These four resonances are assigned to the most likely product, which in a solution containing a tenfold excess of $[^nBu_2SnCl]_2O$ is expected to be the 3:1 (Cl:Br) mixed distannoxane dimer, **I**. In a similar manner the resonances associated with the 1:3 mixed distannoxane dimer, **II**, are identified from the 1:10 mixture: -82.6, -88.5, -131.5 and -141.9 ppm (Fig. 3e). Since the parent dimers and the 3:1 and 1:3 mixed distannoxanes account for 12 of the 20 resonances, the
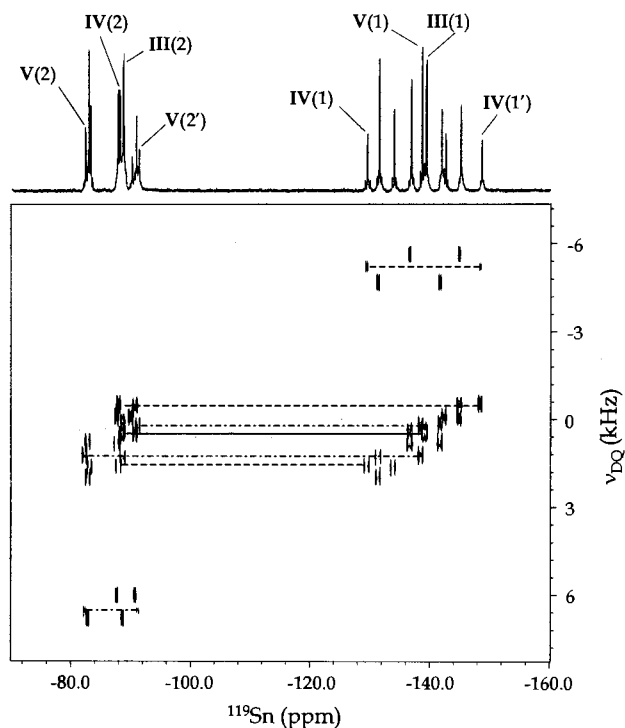
Fig. 4. 111.96 MHz ^{119}Sn 2D INADEQUATE spectrum of the equimolar [^{n}Bu$_2$SnCl]$_2$O/[^{n}Bu$_2$SnBr]$_2$O mixture with [Sn]$_T$ = 2.0 M in benzene-d_6 at 298 K. The experiment was optimized for 60 Hz couplings, τ_{DQ} = 4.17 ms. Lines are drawn to show the coupling network associated with the 2:2 mixed distannoxane dimers, **III** (solid line), **IV** (dashed line) and **V** (dot-dashed line).

Fig. 5. Ladder structures for the mixed distannoxane dimers of the [^{n}Bu$_2$SnCl]$_2$O/[^{n}Bu$_2$SnBr]$_2$O binary system.

remaining eight resonances are attributed to the 2:2 mixed distannoxane dimers. The ^{119}Sn 2D INADEQUATE spectrum of the equimolar mixture (Fig. 4) reveals that these eight signals are due to three 2:2 mixed distannoxane dimers: **III**, − 87.8(1) and − 139.3(1) ppm; **IV**, − 88.4(2), − 129.6(1) and − 148.6(1) ppm; **V**, − 82.1(1), − 91.0(1) and − 139.6(2) ppm. The numbers given in parentheses are the relative number of tin nuclei responsible for each resonance. Thus, the eight 2:2 mixed distannoxane dimer resonances are distributed among **III**, **IV**, and **V** as follows 2:3:3 (**III:IV:V**).

A total of eight possible ladder structures can be drawn to describe the Cl:Br mixed distannoxane dimers (Fig. 5). The ladder structures describing the 3:1, **I** and **I′**, and 1:3 mixed distannoxane dimers, **II** and **II′**, would each produce four tin resonances. Ladder structures **IV** and **V** would each produce four tin resonances; while **III** and **III′** would each contribute a pair of tin resonances to the NMR spectrum. If relative donor ability is determined solely on the basis of electronegativity, then for the Cl:Br mixed distannoxane dimers, the Cl ligand would be expected to preferentially occupy the bridging sites. For the 3:1 and 1:3 mixed distannoxane dimers, preferential Cl bridging would indicate that **I**
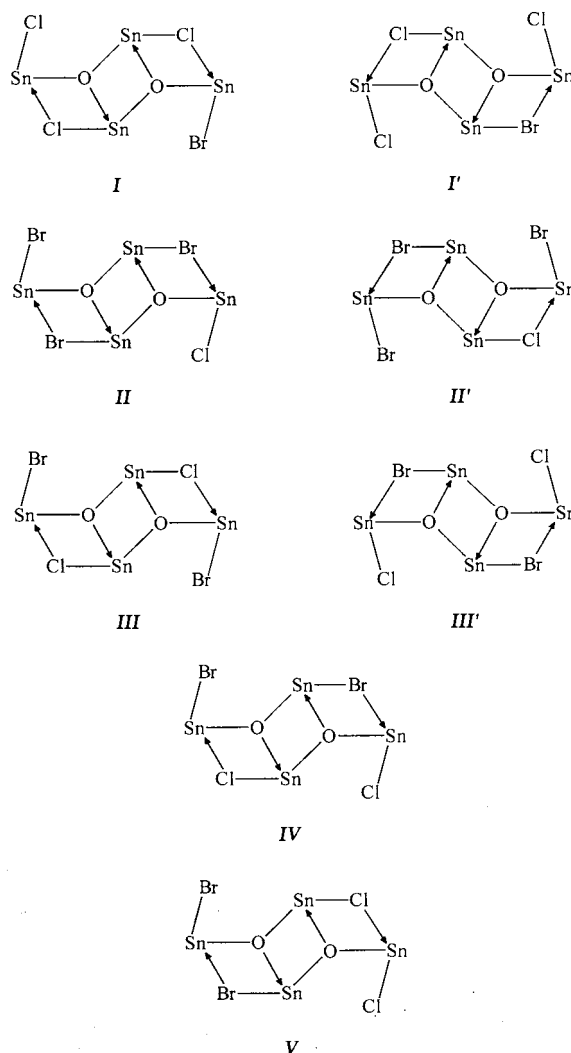
and **II′** are preferred. Although this simple argument would explain the number of observed resonances for the 3:1 and 1:3 mixed distannoxane dimers, it does not reconcile their presence in the equimolar mixture nor does it correctly predict the observed number of 2:2 mixed distannoxane dimers. In fact, no combination of three ladder structures can account for the observed distribution of tin resonances due to the 2:2 mixed distannoxane dimers.

A successful interpretation of the ^{119}Sn-NMR spectral data is achieved using time-averaged ladder structures resulting from the intradimeric distannoxane process. Computer modeling [27] supports the view that this fluxional process proceeds via migration of the bridging and nonbridging bonds coupled with the correlated motion of the tins, oxygens and ligands (Scheme 1). The transition state is characterized by ligands located at positions that are weighted averages of the bridging and nonbridging sites of **I** and **I′**. Rapidly

interconverting ladder structures, $\mathbf{I} \leftrightarrow \mathbf{I}'$, would produce two endocyclic and two exocyclic tin resonances. Similarly, rapid interconversion of the ladder structures
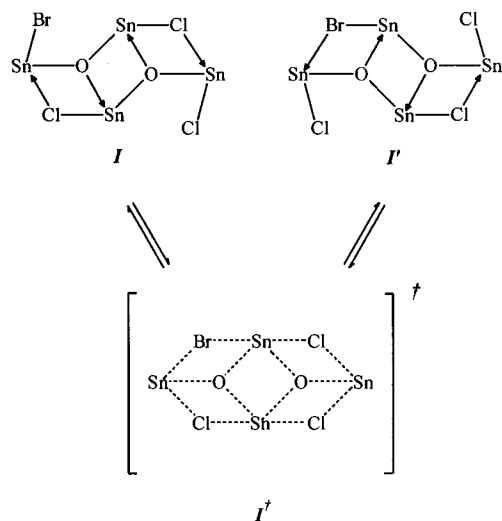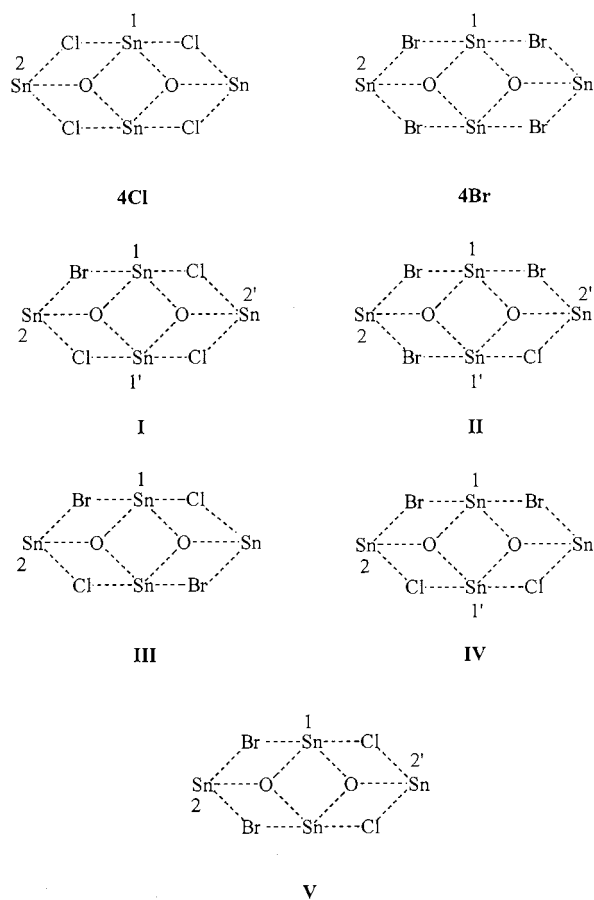

Scheme 1.

Fig. 6. Pictorial representation of the time-averaged dimeric distannoxane structures resulting from the intradimeric distannoxane process, i.e. rapid interconverting ladder pairs.

associated with the 1:3 mixed distannoxane dimer, $\mathbf{II} \leftrightarrow \mathbf{II}'$, and the centrosymmetric 2:2 mixed dimer, $\mathbf{III} \leftrightarrow \mathbf{III}'$, would yield four and two tin resonances, respectively. When this intradimeric distannoxane process occurs in $\mathbf{IV}$ and $\mathbf{V}$, different ladder structures are not produced. However, this fluxional process leads to the mutual exchange of the exocyclic tins of $\mathbf{IV}$ and mutual exchange of the endocyclic tins of $\mathbf{V}$. In the limit of rapid interconversion, the time-averaged structure for $\mathbf{IV}$ yields one exo- and two endocyclic tin resonances; while the time-averaged structure for $\mathbf{V}$ produces one endo- and two exocyclic tin signals. The 16 tin resonances that would be produced by the time-averaged mixed distannoxane dimers agree with the number of observed resonances. In addition, the predicted number of resonances for each of the time-averaged structures is in agreement with the observed distribution of resonances among the mixed distannoxane dimers. The time-averaged structures for the Cl:Br mixed distannoxane dimers, resulting from the rapid interconversion of ladder structures, are represented pictorially in Fig. 6.

Describing the distannoxane dimers as time-averaged ladder structures permits the straightforward assignment of the ^{119}Sn-NMR spectra of the binary [^{n}Bu$_2$SnCl]$_2$O/[^{n}Bu$_2$SnBr]$_2$O system. Assignment of resonances associated with the 3:1 mixed distannoxane dimer, $\mathbf{I}$, is accomplished by comparison with $\{[^{n}$Bu$_2$SnCl]$_2$O$\}_2$ ($\mathbf{4Cl}$). The Sn(2′) environment of $\mathbf{I}$, $\mathbf{I}(2')$, which closely approximates the exocyclic tin sites of $\mathbf{4Cl}$, is assigned to the resonance, located at -90.6 ppm. It follows that the -87.5 ppm resonance is due to $\mathbf{I}(2)$. The chemical shift of $\mathbf{I}(1)$ is expected to be between the chemical shifts observed for the endocyclic tins of $\mathbf{4Cl}$ and $\mathbf{4Br}$. Therefore, the resonances located at -136.8 and -145.1 ppm are assigned to $\mathbf{I}(1)$ and $\mathbf{I}(1')$, respectively. Similarly, comparison of the shifts of $\mathbf{II}$ and $\mathbf{4Br}$ leads to the assignment of the 1:3 mixed distannoxane dimer. Using the chemical shift differences observed between $\mathbf{I}$ and $\mathbf{II}$ the resonances of the 2:2 mixed distannoxane dimers are readily assigned (Table 2).

Attempts to freeze out the intradimeric distannoxane process and obtain individual ladder structures were unsuccessful. The low temperature behavior of the ^{119}Sn-NMR spectrum of the [^{n}Bu$_2$SnCl]$_2$O/[^{n}Bu$_2$SnBr]$_2$O binary system ([Sn]$_T$ = 2.0 M) using a 1:3 CHCl$_3$:CFCl$_3$ solvent system, is shown in Fig. 7. As the temperature is lowered, the linewidths of the tin resonances increase; however, a slight preferential broadening is observed for the endocyclic tins. The observed linewidths of the mixed distannoxane dimers do not broaden significantly compared to the resonances of the parent dimers, $\mathbf{4Cl}$ and $\mathbf{4Br}$. Therefore, the observed broadening of the resonances as the temperature is lowered is due to shortening of the spin–spin relaxation

Table 2
^{119}Sn-NMR spectral parameters of distannoxane dimers present in binary mixtures of [^{n}Bu$_2$SnCl]$_2$O and [^{n}Bu$_2$SnBr]$_2$O

Dimer [c]	^{119}Sn (δ ppm) [a]				$|^nJ(^{119}$Sn, ^{119}Sn$)|$ (Hz) [b]					
	Sn(1)	Sn(1')	Sn(2)	Sn(2')	$^2J(1,1')$	$^2J(1,2)$	$^2J(1,2')$	$^2J(1',2)$	$^2J(1',2')$	$^4J(2,2')$
4Cl	−142.6	(−142.6) [d]	−89.8	(−89.8)	22.4 [e]	73.3	(73.3)	(73.3)	(73.3)	32.5 [e]
4Br	−134.0	(−134.0)	−82.9	(−82.9)	44.4 [e]	80.0	(80.0)	(80.0)	(80.0)	36.1 [e]
I	−136.8	−145.1	−87.5	−90.6	28.9	93.6	70.0	58.4	76.7	33.9
II	−131.5	−141.9	−82.6	−88.5	40.8	79.4	94.1	80.9	58.0	35.8
III	−139.6	(−139.6)	−87.8	(−87.8)	35.0 [e]	96.3	56.3	(56.3)	(96.3)	[f]
IV	−129.6	−148.6	−88.4	(−88.4)	35.5 [e]	90.9	(90.9)	60.1	(60.1)	[f]
V	−139.3	(−139.3)	−82.1	−91.0	35.0 [e]	78.5	76.1	(78.5)	(76.1)	34.2

[a] The chemical shift scale is referenced using an internal shift standard, TMT = 0.0 ppm. The shifts are reported for the equimolar [^{n}Bu$_2$SnCl]$_2$O/[^{n}Bu$_2$SnBr]$_2$O mixture in benzene-d_6 at 298 K with [Sn]$_T$ = 2.0 M. Variations in the chemical shifts due to composition are less than 0.02 ppm.

[b] Unless specified the ^{119}Sn–^{119}Sn couplings were determined from the ^{119}Sn 1D INADEQUATE spectrum acquired on the binary mixtures. The sign of the couplings was not determined. The uncertainty in $^nJ(^{119}$Sn,^{119}Sn$)$ is estimated to be ± 0.4 Hz.

[c] The time-averaged structures and the numbering scheme are depicted in Fig. 6.

[d] Chemical shifts and couplings in parentheses are due to symmetry-related environments.

[e] $^nJ(^{119}$Sn,^{119}Sn$) = ^nJ(^{119}$Sn,^{117}Sn$)[\gamma(^{119}$Sn$)/\gamma(^{117}$Sn$)]$.

[f] Unobservable coupling between magnetically equivalent nuclei, in which $^nJ(^{119}$Sn,^{117}Sn$)$ is not detected due to spectral overlap.

times, T_2, and not the result of slowing the intradimeric distannoxane process.

Integration of the ^{119}Sn-NMR spectrum of the equimolar mixture reveals that the concentrations of the 2:2 mixed distannoxane dimers are equivalent. This result indicates that Cl and Br exhibit nearly identical donor abilities towards tin. The lack of preference for the bridging sites implies that positional ordering of the halogens within the mixed Cl–Br distannoxane dimers does not exist. More importantly, this observation suggests that the redistribution reaction results in a random distribution of the mixed distannoxane dimers. In Fig. 8, the observed concentrations of the distannoxane dimers, as a function of initial [^{n}Bu$_2$SnCl]$_2$O concentration, are compared to the concentrations predicted by a statistical distribution. From the figure, it is clear that the observed concentrations of the distannoxane dimers are well represented by a random distribution of the halogens. A statistical redistribution of the halogens dictates that the concentrations of the individual ladder structures of an interconverting pair, are also equal. Consequently the observed ^{119}Sn and ^{13}C chemical shifts as well as the ^{119}Sn–^{119}Sn scalar couplings are expected to be simple averages of the corresponding ladder values.

3.2. ^{13}C spectrum

Assignment of the ^{13}C-NMR spectrum of the [^{n}Bu$_2$SnCl]$_2$O/[^{n}Bu$_2$SnBr]$_2$O binary system is achieved using the same method employed to assign the ^{119}Sn-NMR spectrum, i.e. varying the relative concentrations of the reactant distannoxanes. The α-carbon region, 32–38 ppm, of the 75.51 MHz ^{13}C-NMR spectrum of the equimolar mixture in benzene-d_6 is shown in Fig. 9.
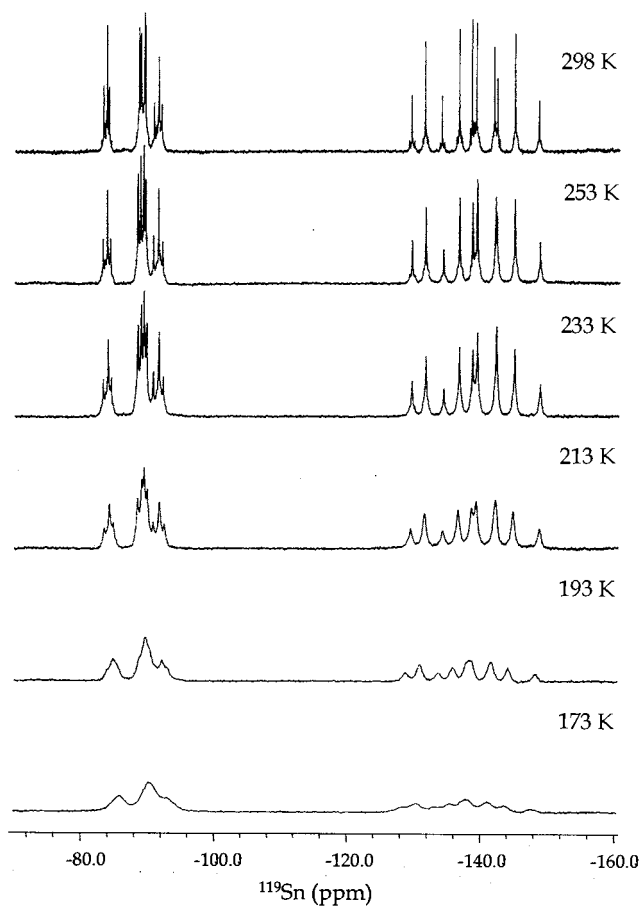

Fig. 7. 111.96 MHz ^{119}Sn-NMR spectrum of the equimolar [^{n}Bu$_2$SnCl]$_2$O/[^{n}Bu$_2$SnBr]$_2$O mixture with [Sn]$_T$ = 2.0 M as a function of temperature. The solvent system is a 1:3 ratio of CHCl$_3$:CFCl$_3$ by volume.
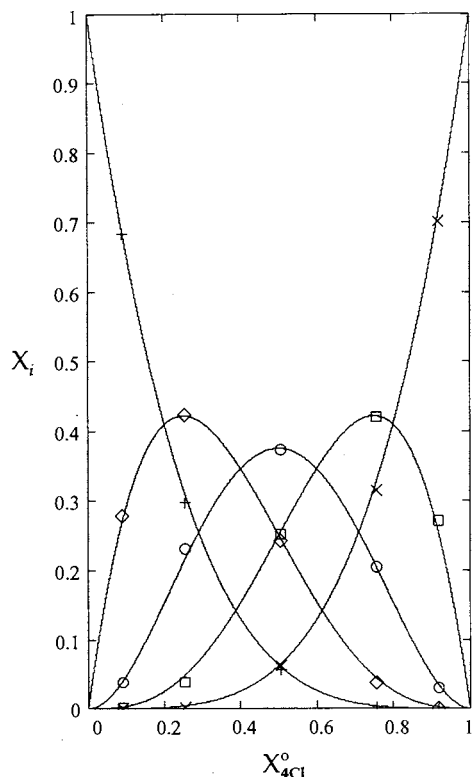
Fig. 8. The observed room temperature concentrations of the distannoxane dimers in the binary mixtures as a function of initial concentration of $\{[^nBu_2SnCl]_2O\}_2$, X^o_{4Cl}: $\times$, X_{4Cl}; $+$, X_{4Br}; $\square$, X_I; $\diamond$, X_{II}; $\bigcirc$, $X_{2:2} = X_{III} + X_{IV} + X_V$; $X_{III} = X_{IV} = X_V$. The curves represent the concentrations predicted by a statistical distribution of the halogens.

The identity of endo- and exocyclic α-carbon environments are confirmed by correspondence to the tin sites using $^1J(^{119}Sn,^{13}C)$ (Table 3). At 298 K, both endocyclic and exocyclic α-carbon resonances of **III** and **IV** as well as the endocyclic α-carbon resonances of **I** and **II** exhibit increased linewidth compared to the other α-carbon resonances. Raising the temperature to 323 K results in chemical shift changes and the preferential broadening of the endocyclic α-carbon resonances of **I**, **II**, **III** and **IV**, while the exocyclic α-carbon resonances of **III** and **IV** narrow. At 348 K the endocyclic α-carbon resonances of **I**, **II**, **III**, and **IV** have sufficiently broadened, nearly disappearing into the baseline. This behavior indicates that an additional fluxional process is occurring in **I**, **II**, **III** and **IV**. Further discussion of this fluxional process is deferred to the following sections.

3.3. Redistribution mechanism

It is generally assumed that ligand redistribution reactions involving metal centers proceed via an intermolecular ligand exchange process resulting from bimolecular collisions in which a four-centered transition state is formed and subsequently undergoes an interchange of the ligands (Scheme 2) [38–41]. However,

when the metal center is tin, there is substantial experimental evidence supporting a halide-catalyzed exchange mechanism [42,70–73]. In this step-wise complex formation process [38], initial dissociation of the dimers in which halide and cationic tin species are liberated, is followed by rapid reassociation of the cationic tin species with a different halide (Scheme 3). In the case of distannoxanes it has been suggested that ligand redistribution occurs via a monomer/dimer mechanism, which relies on the establishment of equilibria between the fluxional dimers and their constituent monomers [24]. In order to explain the reaction products of the $[^nBu_2SnCl]_2O/[^nBu_2SnBr]_2O$ binary system the mono–dimer mechanism must account for the formation of the mixed monomer intermediate, $Cl^nBu_2SnOSn^nBu_2Br$. Using non-fluxional ladder structures, the mixed monomer can be formed only if the reactant monomers, $[^nBu_2SnCl]_2O$ and $[^nBu_2SnBr]_2O$, undergo intermolecular ligand exchange. The combined processes define the multi-step mechanism suggested by Gross [24]. The fluxional description of the distannoxane dimers yields the mixed monomer without resorting to the incorporation of an additional step (Scheme 4). An important feature of both the bimolecular mechanism of Scheme 2
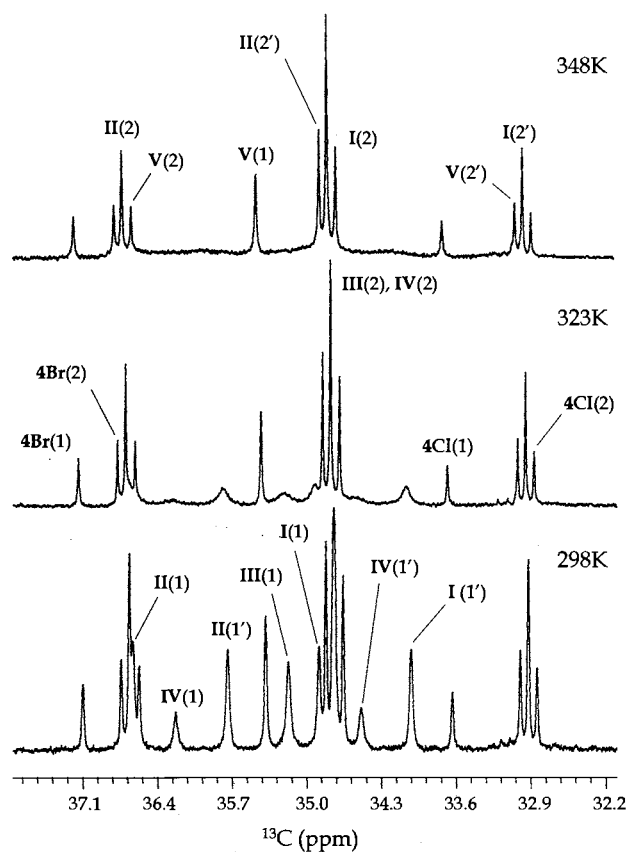

Fig. 9. The α-carbon region of the 75.51 MHz ^{13}C-NMR spectrum of the equimolar $[^nBu_2SnCl]_2O/[^nBu_2SnBr]_2O$ mixture with $[Sn]_T = 2.0$ M in benzene-d_6 as a function of temperature.

Table 3
^{13}C-NMR spectral parameters of distannoxane dimers present in binary mixtures of [^{n}Bu$_2$SnCl]$_2$O and [^{n}Bu$_2$SnBr]$_2$O [a]

Dimer [b]	^{13}C (δ ppm)				$^1J(^{119}$Sn, ^{13}C) (Hz)			
	α-C(1)	α-C(1′)	α-C(2)	α-C(2′)	^1J(1,C)	^1J(1′,C)	^1J(2,C)	^1J(2′,C)
4Cl	33.63	(33.63) [c]	32.84	(32.84)	601	(601)	574	(574)
4Br	37.09	(37.09)	36.74	(36.74)	602	(602)	552	(552)
I	34.87	34.01	34.65	32.92	600	606	562	574
II	36.62	35.73	36.66	34.82	597	607	552	562
III	35.38	(35.38)	34.75	(34.75)	601	(601)	562	(562)
IV	36.22	34.49	34.73	(34.73)	594	610	562	(562)
V	35.38	(35.38)	36.57	33.00	601	(601)	553	574

[a] The chemical shift scale is referenced using an internal shift standard, TMS = 0.0 ppm. The shifts are reported for the equimolar [^{n}Bu$_2$SnCl]$_2$O/[^{n}Bu$_2$SnBr]$_2$O mixture in C$_6$D$_6$ with [Sn]$_T$ = 2.0 M. Variations in the chemical shifts due to composition are less than 0.05 ppm. Uncertainty in $^1J(^{119}$Sn,^{13}C) is estimated to be ± 1 Hz.
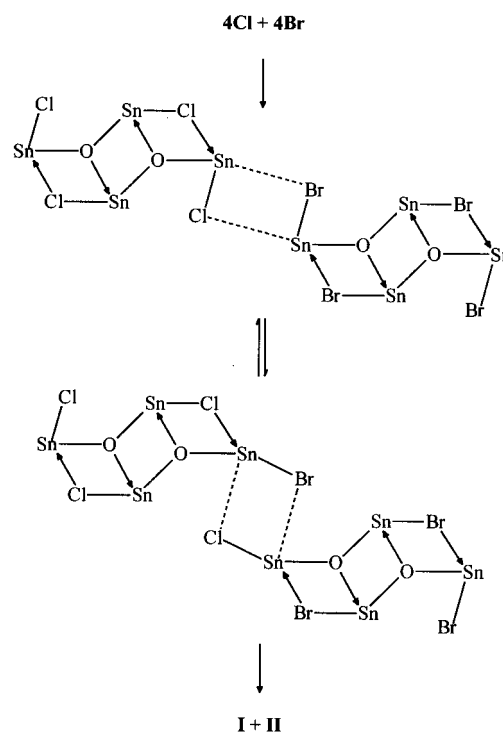
[b] The time-averaged structures and the numbering scheme are depicted in Fig. 6.

[c] Chemical shifts and couplings in parentheses are due to symmetry-related environments.
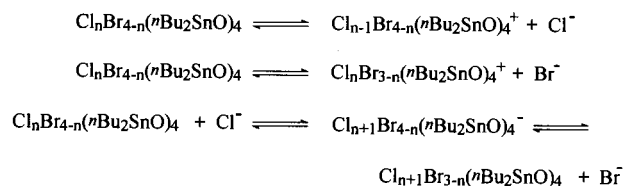
and the halide-catalyzed mechanism of Scheme 3 are single halogen exchanges; whereas, the monomer/dimer mechanism is characterized by the scrambling of endo- and exocyclic tin environments. It must be noted that none of the transient intermediates associated with either the halide-catalyzed process or the monomer/dimer mechanism are detected in the NMR spectrum.

The operative ligand redistribution mechanism is determined with the aid of ^{13}C exchange spectroscopy. The α-carbon region of the ^{13}C EXSY spectrum of the equimolar [^{n}Bu$_2$SnCl]$_2$O/[^{n}Bu$_2$SnBr]$_2$O mixture ([Sn]$_T$ = 2.0 M) acquired using a mixing time of 1 s is shown in Fig. 10. The intermolecular exchange crosspeaks, which are connected by solid lines in the figure, are consistent with the replacement of the ligands one halogen at a time and is indicative of both the bimolecular and the halide catalyzed mechanisms. Crosspeaks between endo- and exocyclic α-carbon environments are not observed confirming that the integrity of the tin sites is maintained during the mixing time of the experiment, τ_m = 1 s. The mixing time used to obtain the ^{13}C EXSY spectrum presented in Fig. 10 is sufficiently long producing crosspeaks consistent with the replacement of two halogens in a single step. These crosspeaks are absent at shorter mixing times, τ_m = 0.5 s, indicating they are produced by an indirect intermolecular exchange, i.e. consecutive single halogen exchanges. Not all of the possible crosspeaks that are dictated by the intermolecular exchange of the halogens are observed. The inability to detect a given crosspeak associated with this process is due to spectral overlap, insufficient concentration of a given dimer and/or the increased linewidths of endocyclic α-carbons of **I**, **II**, **III** and **IV**. The remaining crosspeaks in the ^{13}C EXSY spectrum arise from the mutual exchange of the endocyclic sites of **I** and **II** confirming the presence of an additional intramolecular exchange process.
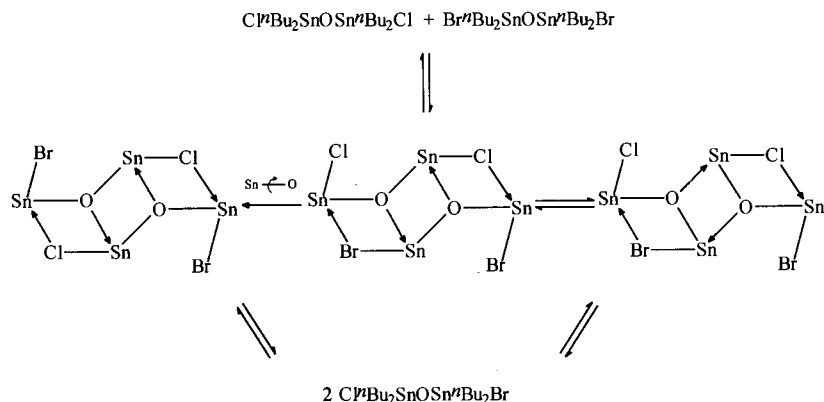
To distinguish between the bimolecular and the halide-catalyzed mechanisms, ^{13}C EXSY spectra were obtained after the addition of iodine. If the operative

Scheme 2.

$$Cl_nBr_{4-n}(^nBu_2SnO)_4 \rightleftharpoons Cl_{n-1}Br_{4-n}(^nBu_2SnO)_4^+ + Cl^-$$

$$Cl_nBr_{4-n}(^nBu_2SnO)_4 \rightleftharpoons Cl_nBr_{3-n}(^nBu_2SnO)_4^+ + Br^-$$

$$Cl_nBr_{4-n}(^nBu_2SnO)_4 + Cl^- \rightleftharpoons Cl_{n+1}Br_{4-n}(^nBu_2SnO)_4^- \rightleftharpoons$$

$$Cl_{n+1}Br_{3-n}(^nBu_2SnO)_4 + Br^-$$

Scheme 3.

$Cl^nBu_2SnOSn^nBu_2Cl$ + $Br^nBu_2SnOSn^nBu_2Br$

2 $Cl^nBu_2SnOSn^nBu_2Br$

Scheme 4.

process for the redistribution of the halogens is the halide-catalyzed mechanism (Scheme 3), it is expected that the addition of iodine would impede the intermolecular exchange by scavenging the halides via formation of complex ions, I_2Br^- and I_2Cl^-. Halogen exchange in the Me_2SnCl_2/Me_2SnBr_2 binary system ($[Cl]_T + [Br]_T = 2.0$ M) is significantly retarded at 0.03 M I_2, slowing the exchange rates by nearly two orders of magnitude [42]. Reduction in the exchange rate would lead to intermolecular exchange crosspeaks with diminished intensities. The presence of halide impurities accelerates the intermolecular exchange of the halogens in dialkyl tin(IV) dihalides [42,74]. Addition of 3.1 mmol of $^nBu_4NBr$ to a 1 ml solution containing an equimolar mixture of Me_2SnCl_2/Me_2SnBr_2 increases the exchange rate by a factor of 30 [42]. In the $[^nBu_2SnCl]_2O/[^nBu_2SnBr]_2O$ binary mixture, it is not known whether or not halide impurities are present. However, it is anticipated that at 0.25 M I_2 excess iodine is present and halide ions resulting from possible impurities would be in the form of complex ions, I_2X^-. With the addition of 23 and 190 mg of iodine ($[I_2] = 0.03$ and 0.25 M, respectively), the intensities of the crosspeaks arising from the intermolecular halogen exchange remained unchanged. Thus, in the $[^nBu_2SnCl]_2O/[^nBu_2SnBr]_2O$ binary system, intermolecular halogen exchange occurs via the bimolecular mechanism (Scheme 2).

3.4. Intramolecular halogen exchange

A more complete picture of the intramolecular exchange process responsible for the broadening of the endocyclic α-carbon resonances, is obtained from the ^{119}Sn EXSY spectrum of the equimolar $[^nBu_2SnCl]_2O/[^nBu_2SnBr]_2O$ mixture. The ^{119}Sn EXSY spectrum (Fig. 11) exhibits six crosspeak pairs. The crosspeaks located at $(-136.8, -145.1)$ and $(-131.5, -141.9)$ as well as their symmetrical partners, are due to the mutual exchange of the endocyclic tins of **I** and **II**, respectively.

The three crosspeaks observed at $(-139.3, -148.6)$, $(-129.6, -139.3)$, and $(-87.8, -88.4)$ and the associated symmetrical crosspeaks are evidence for the interconversion of **III** and **IV**. The remaining crosspeak pair, $(-129.6, -148.6)$ and $(-148.6, -129.6)$, is due to a two-step exchange process that results in the mutual exchange of the endocyclic sites of **IV**. This intramolecular exchange process, which occurs via rotation of the oxygen–exocyclic tin bond results in the
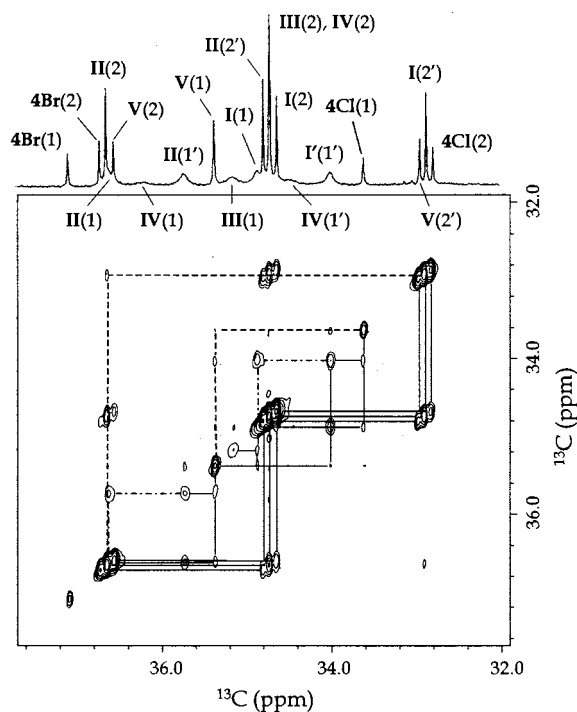

Fig. 10. The α-carbon region of the 75.51 MHz ^{13}C EXSY spectrum of the equimolar $[^nBu_2SnCl]_2O/[^nBu_2SnBr]_2O$ mixture with $[Sn]_T = 2.0$ M in benzene-d_6 at 328 K, acquired with $\tau_{mix} = 1.0$ s. Intermolecular exchange crosspeaks are connected with solid lines, while dashed lines connect crosspeaks arising from an indirect (two-step) intermolecular halogen exchange. Crosspeaks resulting from an intramolecular process are connected with dot–dash lines, see text.
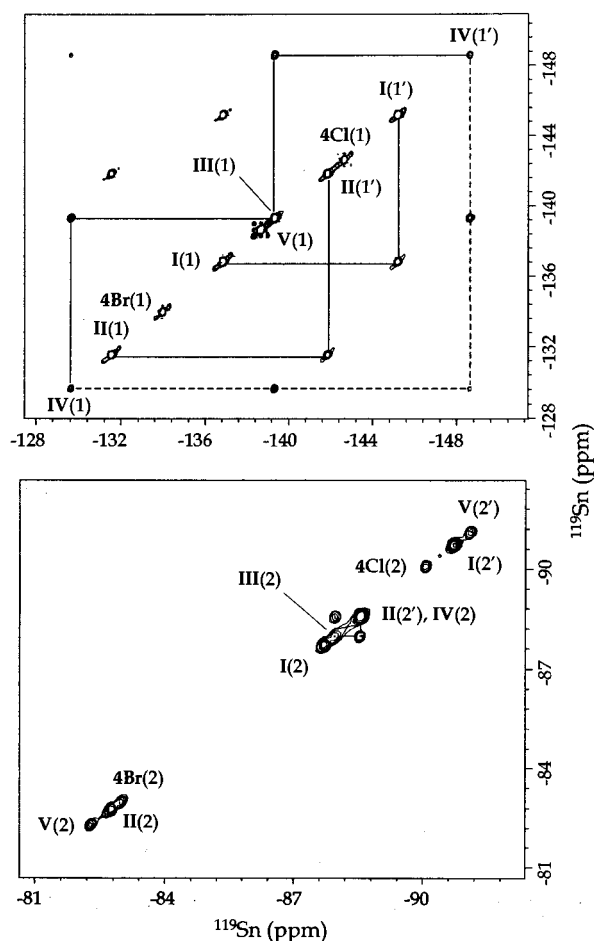
Fig. 11. 111.96 MHz ^{119}Sn EXSY spectrum of the equimolar [^{n}Bu$_2$SnCl]$_2$O/[^{n}Bu$_2$SnBr]$_2$O mixture with [Sn]$_T$ = 2.0 M in benzene-d_6 at 318 K, acquired with τ_{mix} = 75 ms. Crosspeaks connected with solid lines are due to the reversible configurational rearrangement, i.e. rotation of the exocyclic tin–oxygen bond. An indirect (two-step) exocyclic tin–oxygen bond rotation gives rise to the exchange of the endocyclic tins of IV (dashed line).
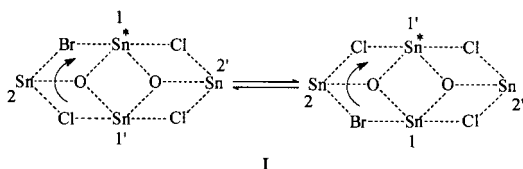
Scheme 5.

interchange of the halogens directly bound to the same exocyclic tin (Scheme 5). This fluxional process is the reversible analog to the configurational rearrangement proposed by Michel and coworkers [27]. Initially, Sn* is in a Sn(1) environment with different pendent halogens. Rotation of the oxygen–exocyclic tin bond swaps the halogens of Sn(2), causing the environments of Sn(1) and Sn(1′) to interchange. This reversible process is not

only responsible for the mutual exchange of the endocyclic sites of I and II, but it also leads to the interconversion of III and IV. When rotation of the oxygen–exocyclic tin bond results in the interchange of like halogens, as in 4Cl, 4Br, I, II and V, the NMR spectra are unaffected.

Analysis of the ^{119}Sn EXSY spectrum yields the rate constants for the oxygen–exocyclic tin bond rotation. The rate constants are a measure of the rate of magnetization transfer from one tin site to another. In the case of the mutual exchange of the endocyclic tins of I and II, the observed rate constants are a direct measure of the rate of rotation about an oxygen–exocyclic tin bond. However, the observed rate of magnetization transfer between the exocyclic tins of III and IV, is twice the rate of oxygen–exocyclic tin bond rotation. The factor of two is a result of multiple magnetization transfer pathways, i.e. rotation about either oxygen-exocyclic tin in III and IV bond leads to interconversion. The measured rates of the oxygen–exocyclic tin bond rotation are presented in Table 4. It is observed that the rate of bond rotation is nearly three times faster in chloroform-d than in benzene-d_6. At room temperature the rate constants for dimers III and IV, which are rotational isomers of each other, are equal. As the temperature is increased a divergence in the rate of bond rotation for III and IV is observed, such that $k(IV) > k(III)$. This divergence indicates that at elevated temperatures, there is a slight shift in the equilibrium favoring isomer III. At 348 K, in benzene-d_6, the concentration ratio between III and IV is found to be [III]/[IV] = 1.12 ± 0.06. However, due to spectral overlap, this equilibrium shift could not be detected by integration of the quantitative spectrum. In benzene-d_6 the Gibbs free energy of activation at 298 K, $\Delta G^{\ddagger}_{298}$, is approximately 70.8 kJ mol^{-1}; while $\Delta G^{\ddagger}_{298}$ is observed to be approximately 2.7 kJ mol^{-1} lower in chloroform-d. In the same solvent and over the narrow temperature range studied, E_A and $\Delta H^{\ddagger}$ are approximately equal for each dimer. However, for each dimer the activation parameters, E_A and $\Delta H^{\ddagger}$, are smaller in chloroform-d compared to those obtained in benzene-d_6, indicating that the activation barrier for oxygen–exocyclic tin bond rotation is lower in chloroform-d than in benzene-d_6.

4. Conclusions

The dimeric ladder structure, which the tetraorganodistannoxanes are known to adopt in the solid phase, is retained in noncoordinating solvents. Dimers of [R$_2$SnXY]$_2$O in which the X and Y ligands are the same or exhibit similar donor abilities toward tin, rapidly rearrange in solution by an intradimeric process. This

Table 4
Rate of oxygen–exocyclic tin bond rotation in mixed Cl:Br distannoxane dimers [a]

Temperature (K)	Rate constant (s^{-1}) [b]							
	Solvent:benzene-d_6				Solvent:$CDCl_3$			
	$k(I)$	$k(II)$	$k(III)$	$k(IV)$	$k(I)$	$k(II)$	$k(III)$	$k(IV)$
298	2.26 ± 0.09	2.62 ± 0.12	2.45 ± 0.10	2.55 ± 0.07	6.70 ± 0.40	7.73 ± 0.65	7.51 ± 0.58	7.50 ± 0.57
308	5.83 ± 0.40	6.93 ± 0.22	5.84 ± 0.28	6.10 ± 0.21	14.0 ± 1.0	14.9 ± 1.1	14.5 ± 1.1	15.4 ± 1.2
318	12.9 ± 0.7	13.7 ± 0.9	12.2 ± 0.9	12.9 ± 0.8	28.7 ± 1.8	31.0 ± 1.9	26.7 ± 1.8	30.2 ± 1.8
328	25.7 ± 1.5	25.9 ± 1.5	25.4 ± 1.5	27.8 ± 1.6	55.9 ± 2.8	63.2 ± 2.9	46.1 ± 2.2	52.4 ± 2.7
338	47.5 ± 2.6	57.8 ± 2.7	45.3 ± 2.4	48.1 ± 2.7	95.2 ± 4.4	109 ± 8	79.1 ± 3.8	91.8 ± 4.7
348	86.2 ± 3.7	104 ± 7	78.3 ± 2.4	87.8 ± 3.8				
E_A (kJ mol^{-1})	57 ± 4	59 ± 5	53 ± 4	55 ± 4	53 ± 4	54 ± 4	47 ± 4	49 ± 4
$\Delta H^\dagger$ (kJ mol^{-1})	53 ± 4	57 ± 5	50 ± 4	52 ± 4	51 ± 4	52 ± 5	45 ± 4	47 ± 4
$\Delta S^\dagger$ (J mol^{-1})	-57 ± 13	-46 ± 14	-66 ± 14	-59 ± 14	-58 ± 14	-53 ± 13	-78 ± 14	-70 ± 14
$\Delta G^\dagger_{298}$ (kJ mol^{-1})	71.0 ± 0.1	70.6 ± 0.1	70.8 ± 0.2	70.7 ± 0.1	68.3 ± 0.2	67.9 ± 0.2	68.0 ± 0.2	68.0 ± 0.2

[a] Rate constants are determined for solutions with $[Sn]_T = 2.0$ M.

[b] Reported errors are estimates of the 95% confidence level.

fluxional process involves interconverting ladder structure that proceeds via migration of the bridging and nonbridging bonds coupled with motion of the atoms that define the ladder structure. The ladder structure is also capable of undergoing an additional intramolecular fluxional process, involving rotation about the oxygen–exocyclic tin bond. When either ligand exhibits significantly higher donor ability towards tin, these dynamic processes do not occur resulting in a frozen dimer with the better donor ligand occupying the bridging sites. The difference in donor abilities also accounts for the composition of binary mixtures containing dissimilar monofunctional distannoxanes, $[R_2SnX]_2O$ and $[R_2SnY]_2O$. Depending on the relative donor abilities of the X and Y ligands, the equilibrium composition of the equimolar mixture ranges from a statistical distribution of X:Y mixed distannoxane products to a single 2:2 mixed dimer in which the bridging sites are occupied by the better donor ligand.

References

[1] S. Matsuda, H. Matsuda, A. Ninagawa, N. Iwamoto, Kogyo Kagaku Zasshi 71 (1968) 2054.

[2] K. Itoi, Japan Pat. 46,006,431.

[3] (a) J. Otera, T Yano, R. Okawara, Organometallics 5 (1986) 1167. (b) M. Yokoo, A. Keshi, N. Hashimoto, S. Nakahara, U.S. Pat. 3,681,271. (c) K. Treadwell, E. Bossert, U.S. Pat. 4,312,959. (d) I. Descheres, Q.T. Pham, Makromol. Chem. 188 (1987) 1909. (e) I. Descheres, Q.T. Pham, Makromol. Chem. 191 (1990) 891.

[4] (a) Y. Hori, A. Suzuki, T. Yamaguchi, T. Nishishita, Macromolecules 26 (1993) 5533. (b) J.E. Kemnitzer, S.P. McCarthy, R.A. Gross, Macromolecules 26 (1993) 6143.

[5] R.J. Chadha, K.C. Panda, U.S. Pat. 3,664,997.

[6] (a) J. Otera, Japan Pat. 62,087,248; 63,041,436 and 63,041,437. (b) J. Otera, T. Yano, A. Kawabata, H. Nozaki, Tetrahedron Lett. 27 (1986) 2383. (c) J. Otera, H. Nozaki, Tetrahedron Lett. 27 (1986) 5743. (d) J. Otera, N. Dan-Oh, H. Nozaki, J. Chem. Soc. Chem. Commun. 24 (1991) 1742. (e) T. Carofiglio, D. Marton, D. Stivanello, G. Tagliavini, Main Group Met. Chem. 15 (1992) 247. (f) D. Marton, D. Stivanello, G. Tagliavini, Gazz. Chim. Ital. 124 (1994) 265.

[7] (a) G.H. Hu, Y.J. Sun, M. Lambla, Makromol. Chem. Phys. 194 (1993) 665. (b) P. Cassagnau, M. Bert, V. Verney, A. Michel, Polymer 34 (1993) 124. (c) J. Bonetti, C. Gondard, R. Pétiaud, M.F. Lauro, A. Michel, J. Organomet. Chem. 481 (1994) 7. (d) A. Legros, P.J. Carreau, B.D. Favis, A. Michel, Polymer 35 (1994) 758. (e) I. Epinasse, R. Pétriaud, M.F. Lauro, A. Michel, Int. J. Polym. Anal. Char. 1 (1995) 137. (f) C. Lacroix, M. Bousmina, P. Carreau, M.F. Llauro, R. Pétiaud, A. Michel, Polymer 37 (1996) 2949. (g) I. Pesneau, M.F. Llauro, M. Gregoire, A. Michel, J. Appl. Polym. Sci. 65 (1997) 2457.

[8] (a) L.R. Sherman, F. Huber, Appl. Organomet. Chem. 2 (1988) 65. (b) R. Barbier, Inorg. Chim. Acta 191 (1992) 253.

[9] (a) M. Bouâlam, R. Willem, M. Biesemans, B. Mahieu, J. Meunier-Piret, M. Gielen, Main Group Met. Chem. 14 (1991) 41. (b) M. Bouâlam, R. Willem, M. Biesemans, M. Gielen, Appl. Organomet. Chem. 5 (1991) 497. (c) M. Gielen, J. Meunier-Piret, M. Biesemans, R. Willem, A. El Khloufi, Appl. Organomet.

Chem. 6 (1992) 59. (d) M. Gielen, A. El Khloufi, M. Biese-
mans, B. Mahieu, R. Willem, Bull. Soc. Chim. Belg. 101 (1992)
243. (e) M. Gielen, A. El Khloufi, M. Biesmenas, R. Willem,
Polyhedron 11 (1992) 1861. (f) M. Gielen, A. El Khloufi, M.
Biesemans, R. Willem, Appl. Organomet. Chem. 7 (1993) 119.
(g) M. Gielen, A. El Khloufi, M. Biesemans, F. Kayser, R.
Willem, Appl. Organomet. Chem. 7 (1993) 201. (h) M. Gielen,
M. Biesemans, A. El Khoufi, J. Meunier-Piret, F. Kayser, R.
Willem, J. Fluorine Chem. 64 (1993) 279. (i) M. Gielen, A.
Bouhdid, R. Willem, V.I. Bregadze, L.V. Ermanson, E.R.T.
Tiekink, J. Organomet. Chem. 501 (1995) 277. (j) M. Gielen,
E.R.T. Tiekink, A. Bouhdid, D. de Vos, M. Biesemans, I.
Verbruggen, R. Willem, Appl. Organomet. Chem. 9 (1995) 639.
[10] G. Lamb, U.S. Pat. 3,632,770.
[11] D.L. Alleston, A.G. Davies, B.N. Figgis, Proc. Chem. Soc.
(1961) 457.
[12] D.L. Alleston, A.G. Davies, M. Hancock, R.F.M. White, J.
Chem. Soc. (1963) 5469.
[13] D.L. Alleston, A.G. Davies, M. Hancock, J. Chem. Soc. (1964)
5744.
[14] W.J. Considine, J.J. Ventura, J. Org. Chem. 28 (1963) 221.
[15] W.J. Considine, J.J. Ventura, A.J. Gibbons, Jr., A. Ross, Can.
J. Chem. 41 (1963) 1239.
[16] R. Okawara, Proc. Chem. Soc. (1961) 383.
[17] R. Okawara, M. Wada, J. Organomet. Chem. 1 (1963) 81.
[18] M. Wada, M. Nishino, R. Okawara, J. Organomet. Chem. 3
(1965) 1342.
[19] Y. Maeda, R. Okawara, J. Organomet. Chem. 10 (1967) 247.
[20] M. Wada, R. Okawara, J. Organomet. Chem. 8 (1967) 261.
[21] A.G. Davies, L. Smith, P.J. Smith, W. McFarlane, J.
Organomet. Chem. 29 (1971) 245.
[22] J. Otera, T. Yano, K. Nakashima, R. Okawara, Chem. Lett.
(1984) 2109.
[23] T. Yano, K. Nakashima, J. Otera, R. Okawara, Organometal-
lics 4 (1985) 1501.
[24] D. Gross, Inorg. Chem. 28 (1989) 2355.
[25] V.K. Jain, V.B. Mokal, P. Sandor, Magn. Reson. Chem. 30
(1992) 1158.
[26] V.B. Mikol, V.K. Jain, J. Organomet. Chem. 441 (1992) 215.
[27] O. Primel, M.F. Llauro, R. Pétiaud, A. Michel, J. Organomet.
Chem. 558 (1998) 19.
[28] C. Vasta, V.K. Jain, T. Kesavadas, E.R.T. Tielink, J.
Organomet. Chem. 408 (1991) 157.
[29] C. Vasta, V.K. Jain, T.K. Das, E.R.T. Tiekink, J. Organomet.
Chem. 418 (1991) 329.
[30] E.R.T. Tiekink, M. Gielen, A. Bouhid, M. Biesemans, R.
Willem, J. Organomet. Chem. 494 (1995) 247.
[31] D. Daternieks, K. Jurkschat, S. van Dreumel, E.R.T. Tiekink,
Inorg. Chem. 36 (1997) 2023.
[32] F. Ribot, C. Sanchez, A. Meddour, M. Gielen, E.R.T. Tiekink,
M. Biesemans, R. Willem, J. Organomet. Chem. 552 (1998)
177.
[33] P.G. Harrison, M.J. Begley, K.C. Molloy, J. Organomet.
Chem. 186 (1980) 213.
[34] J.F. Vollano, R.O. Day, R.R. Holmes, Organometallics 3
(1984) 745.
[35] D. Dakternieks, R.W. Gable, B.F. Hoskins, Inorg. Chim. Acta
85 (1984) L43.
[36] (a) R. Okwara, N. Kasai, K. Yasuda, Second International
Symposium on Organometallic Chemistry, Wisconsin, 1965, p.
128. (b) Y.M. Chow, Inorg. Chem. 10 (1971) 673. (c) H. Mat-
suda, F. Mori, A. Kashiwa, S. Matsuda, N. Kasai, K. Jit-
sumori, J. Organomet. Chem. 34 (1972) 341. (d) C.D. Garner,
B. Hughes, Inorg. Nucl. Chem. Lett. 12 (1976) 859. (e) R.
Graziani, G. Bombieri, F. Forselinni, P. Furlan, V. Peruzzo, G.
Tagliavini, J. Organomet. Chem. 125 (1977) 43. (f) R. Faggiani,
J.P. Johnson, I.D. Brown, T. Birchall, Acta Crystallogr., Sect.

B 34 (1978) 3743. (g) H. Puff, E. Friedrichs, F. Visel, Z. Anorg.
Allg. Chem. 477 (1981) 50. (h) R. Graziani, U. Castellato, G.
Plazzonga, Acta Crystallogr., Sect. C 39 (1983) 1188. (i) H.
Puff, I. Bung, E. Friedrichs, A. Jansen, J. Organomet. Chem.
254 (1983) 23. (j) V. Chandresekhar, R.O. Day, J.M. Holmes,
R.R. Holmes, Inorg. Chem. 27 (1988) 958. (k) S.P. Narula,
S.K. Bharadwaj, H.K. Sharma, G. Mairess, P. Barbier, G.
Nowogrocki, J. Chem. Soc. Dalton Trans. (1988) 1719. (l) G.K.
Sandhu, N. Sharma, E.R.T. Tielink, J. Organomet. Chem. 371
(1989) C1. (m) C.S. Parulekar, V.K. Jain, T.K. Das, A.R.
Gupta, B.F. Hoskins, E.R.T. Tielink, J. Organomet. Chem. 372
(1989) 193. (n) N.A. Alcock, S.M. Roe, J. Chem. Soc. Dalton
Trans. (1989) 1589. (o) E.R.T. Tiekink, Appl. Organomet.
Chem. 5 (1991) 1.
[37] T.P. Lockhart, W.F. Manders, E.M. Holt, J. Am. Chem. Soc.
108 (1986) 6611.
[38] J.C. Lockhart, Chem. Rev. 65 (1965) 131.
[39] K. Moedritzer, Organomet. Chem. Rev. 1 (1966) 179.
[40] K. Moedritzer, in: F.G.A. Stone, R. West (Eds.), Advances in
Organometallic Chemistry, vol. 6, Academic Press, New York,
1968, p. 172.
[41] K. Moedritzer, in: E.I. Becker, M. Tsutsui (Eds.), Organometal-
lics Reactions, vol. 2, Wiley-Interscience, New York, 1971.
[42] S.O. Chan, L.W. Reeves, J. Am. Chem. Soc. 95 (1973) 673.
[43] P. Pfeifer, S. Sergiewskaja, Z. Anorg. Allg. Chem. 68 (1910)
102.
[44] S. Matsuda, H. Matsuda, Kogyo Kaqaku Zasshi 63 (1960) 114.
[45] HBA 1.2, K. Eichele, R.E. Wasylishen, Dalhousie University.
[46] J. Herzfeld, A.E. Berger, J. Chem. Phys. 73 (1980) 6021.
[47] C.L. Perrin, R.K. Gipe, J. Am. Chem. Soc. 106 (1984) 4036.
[48] J.W. Keepers, T.L. James, J. Magn. Reson. 57 (1984) 404.
[49] J. Bremer, G.L. Mendz, W.J. Moore, J. Am. Chem. Soc. 106
(1984) 4691.
[50] E.T. Olejiniczak, R.T. Gampe, Jr., S.W. Fesik, J. Magn. Reson.
67 (1986) 28.
[51] C.L. Perrin, T.J. Dwyer, Chem. Rev. 90 (1990) 935.
[52] C.L. Perrin, J. Magn. Reson. 82 (1989) 619.
[53] P.W. Kuchel, B.T. Bulliman, B.E. Chapman, G.L. Mendz, J.
Magn. Reson. 76 (1988) 136.
[54] J. Mason, Solid State NMR 2 (1993) 285.
[55] U. Haeberlen, in: J.S. Waugh (Ed.), Advances in Magnetic
Resonance, Academic Press, New York, 1976.
[56] R.K. Harris, A. Sebald, J. Organomet. Chem. 331 (1987) C9.
[57] R.K. Harris, A. Sebald, Magn. Reson. Chem. 25 (1987) 1058.
[58] R. Komoroski, G. Parker, A.M. Mazany, J. Magn. Reson. 73
(1987) 389.
[59] T. Tanaka, Organomet. Chem. Rev. A 5 (1970) 1.
[60] K.C. Molloy, K. Quill, J. Chem. Soc. Dalton Trans. (1985)
417.
[61] D. Karpovich, D.L. Tierney, P.J. Moehs, D.L. Hasha, Ab-
stracts of Papers, 203rd National Meeting of the American
Chemical Society, San Francisco, CA; American Chemical Soci-
ety, Washington, DC, 1992; CHED113.
[62] T.P. Lockhart, J. Organomet. Chem. 287 (1985) 179.
[63] J.A. Pople, D.P. Santry, Mol. Phys. 8 (1964) 1.
[64] T.N. Mitchell, J. Organomet. Chem. 59 (1973) 189.
[65] J. Holeček, M. Nádvoník, K. Handlíř, A. Lyčka, J. Organomet.
Chem. 241 (1983) 177.
[66] J. Holeček, M. Nádvoník, K. Handlíř, A. Lyčka, J. Organomet.
Chem. 275 (1984) 43.
[67] J. Holeček, A. Lyčka, Inorg. Chim. Acta 118 (1986) L17.
[68] J. Holeček, M. Nádvorník, K. Handíř, J. Organomet. Chem.
315 (1986) 299.
[69] T.P. Lockhart, W.F. Manders, J.J. Zuckerman, J. Am. Chem.
Soc. 107 (1985) 4546.
[70] A.K. Sawyer (Ed.), Organotin Compounds, vols. I–III, Marcel
Dekker, New York, 1971.

[71] W.P. Neumann, Organic Chemistry of Tin, Interscience, London, 1970.

[72] R.C. Poller, Chemistry of Organotin Compounds, Logos, London, 1970.

[73] V. Gutmann (Ed.), Halogen Chemistry, vols. I–III, Academic Press, New York, 1967.

[74] E.A. Allan, M.G. Hogben, L.W. Reeves, K.N. Shaw, J. Pure Appl. Chem. 32 (1972) 9.